Kirkuk Journal of Science Vol. 21, Iss. 2, p. 40-52, 2026 doi:10.32894/kujss.2026.170877.1317

Effect of Co:Fe Ratio on Phase Transformations, Structural, Magnetic and Antibacterial Properties of $Co_xFe_{3x}O_4$ Nanocompounds Synthesized by Co-precipitation

Thaer Q. Jasim *, Qahtan. N. Abdullah

Department of Physics, College of Education for Pure Science, Tikrit University, Tikrit, Iraq.
*Corresponding author : thairr112@gmail.com.

Article Information

Article Type:
Research Article

Keywords:
Fe_2o_3 Phases Antibacterial Co_3O_4 *E. coli.*

History:
Received: 16 April 2026
Revised: 9 June 2026
Accepted: 10 June 2026
Available Online: 30 June 2026

Citation: Thaer Q. Jasim, Qahtan. N. Abdullah, Effect of Co:Fe Ratio on Phase Transformations, Structural, Magnetic and Antibacterial Properties of $Co_xFe_{3x}O_4$ Nanocompounds Synthesized by Co-precipitation, Kirkuk Journal of Science, 21(2), p. 40-52, 2026, https://doi.org/10.32894/kujss.2026.170877.1317

Abstract

In this study, fine $Co_3Fe_{3x}O_4$ nanoparticles with cobalt concentrations ($0.2 \leq x \leq 0.8$) were synthesized using a simple one-step co-precipitation method. The effects of cobalt substitution were studied using X-ray diffraction (XRD), field emission scanning electron microscopy (FESEM), energy dispersive X-ray spectroscopy (EDX), Fourier transform infrared spectroscopy (FTIR), and vibrating sample magnetometry (VSM). The synthetic results revealed the formation of a cubic spinel structure at medium concentrations, with crystals ranging from 14 to 21 nm, accompanied by the formation of secondary phases, including hematite (α-Fe_2O_3) and cobalt oxide (CoO/Co_3O_4). EDX examination confirmed the elemental composition and uniform distribution of the constituent elements, whereas (FTIR) spectra validated the distinctive metal–oxygen vibrations of the spinel structure. The chemical composition and crystal structure showed that saturation magnetization values ranged from 0.109 to 2.51 emu g-1. The samples exhibited soft magnetic behavior, which is attributed to the nanoscale effect. The nanoparticles exhibited antibacterial activity with an inhibition zone diameter of 25 mm against *S. aureus* and *E. coli*, which enhances their use in technical and medical applications.

1. Introduction:

Due to their distinctive electrical, magnetic, and architectural properties as well as their wide range of biological and industrial applications, spinel ferrite nanoparticles (SFNs) have recently obtained significant attention in both basic and applied research [1]. It is critical to have a comprehensive understanding that the crystal structure of these materials is strongly influenced by the production technique, which in turn affects their chemical and physical qualities. In most nanomaterials, spinel ferrites with the chemical formula MFe_2O_4 (where M = Mn, Fe, Ni, Cu, Co, or Zn) frequently exhibit superparamagnetic behavior when their diameter is approximately 20 nm or less [1], [2]. Both tetrahedral (A), and octahedral (B) sites have a distribution of metal cations. The stability energy, cationic radius, interstitial site size, synthesis technique, and reaction conditions all affect this distribution [1], [2].

Magnetic nanoparticles possess unique properties that improve their performance compared to solid materials, owing to their substantial surface area per unit volume. Superparamagnetic, magnetic spin deflection, high-field irreversibility, dislocations, and surface anisotropies are among these features [3]. Moreover, through material design, these characteristics make them optimal for particular uses [4]. Cobalt ferrite, a cubic spinel type, has attracted a great deal of study interest among the many magnetic nanoparticles because of its outstanding

characteristics, which include medium saturation magnetization (Ms) and strong coercivity (Hc) [5], [6] In addition, it exhibits strong magnetic anisotropy (380 kJ m^3) [7], high magnetic permeability [8], enhanced mechanical strength, excellent chemical stability, and low production cost [9]. These advantages make cobalt ferrite a key choice for developing new substances used in cell freezing. ceramic materials, devices that use magneto-optics [10], sensors for measuring torque without contact [11], various types of sensors, rods used for antennas [10], devices that create movement [12], materials that respond to light and magnetism [13], as well as uses in healthcare, such as heat treatment [5] and absorbers for microwaves [9], imaging methods like magnetic resonance imaging (MRI) and medication delivery [14].

Particle size, shape, purity, and crystalline magneto-crystalline anisotropy are some of the variables that affect the magnetization of $CoFe_2O_4$ nanoparticles [15]. One of the most important magnetic phenomena observed in ferrite nanoparticles is superparamagnetic behavior. When a magnetic field is applied to $CoFe_2O_4$ nanoparticles, the coercivity decreases to zero, indicating that the nanoparticles become superparamagnetic. Upon the removal of the applied magnetic field, the nanoparticles return to a non-magnetic condition [16]. There are various methods for manufacturing nanoparticles, and among these, co-precipitation is the most efficient method for producing nano ferrites in large quantities because it yields particles with a uniform structure. Co-precipitation is a simple and inexpensive method, as the size and dispersion of the nanoparticles can be controlled by maintaining their formation and growth rates during the process [16], [17].

In this context, Dippong et al. reported the synthesis of the $Co_xFe_{3-x}O_4$ oxidic system via a redox process sing various Fe/Co ratios, leading to the acquisition of cobalt ferrite nanocrystallites. In samples with abundant iron, cobalt ferrite and iron oxides (Fe_2O_3) were produced, but in samples with excess cobalt, cobalt oxides (CoO) emerged as a secondary phase and the synthesized nanomaterials exhibited particle sizes below 100 nm. [18].

Furthermore, Gheidari et al. showed that synthesized nanoparticles inhibit bacterial growth against E. coli and S. aureus. While increasing the nanoparticle concentration improves their antimicrobial properties, resulting in a larger inhibition zone (18-13 mm) [19].

Similarly, Bhushan et al. investigated the antibacterial efficacy of innovative iron oxide and cobalt oxide nanoparticles against *S. aureus* and *E. coli.* The enhanced activity of the iron oxide/cobalt oxide nanoparticle complex resulted from the synergistic effect of these nanoparticles, showing an inhibitory zone diameter of 10–11 mm [20].

Prior studies have addressed structural, magnetic, or biological properties separately, but have not clearly demonstrated how phase development, including secondary phases such as (α-Fe_2O_3 and Co_3O_4), directly influences functional performance of the synthesized nanoparticles. The range $0.2 \le x \le 0.8$ was chosen to examine the compositional transition region where the pure spinel phase competes with secondary phases. This regime has not been systematically investigated in prior research.

This study investigates the influence of cobalt content on phase evolution and identifies the conditions that stabilize the pure spinel phase $Co_xFe_{3-x}O_4$), relative to secondary phases, as the Co/Fe ratio varies. A systematic analysis of the compositional dependence over the range ($0.2 \le x \le 0.8$) yields comprehensive correlations among structure, magnetic properties, and antibacterial activity.

In this study, $Co_xFe_{3-x}O_4$-based nanoparticles were produced using the co-precipitation method, and the effect of four different concentrations ($0.2 \le x \le 0.8$) was observed. The results of the analyses were examined with respect to crystal size, lattice coefficient, saturation magnetization, retention, and magnetic force. $CoxFe_{3x}O_4$-based nanoparticles were evaluated for antibacterial activity against particular pathogens using the agar diffusion method.

2. Experimental part:

2.1 Sample synthesis:

The starting precursors were $Co(NO_3)_2{\cdot}6H_2O$, $FeCl_3$ deionized water, and NH_4OH. $CoFe_2O_4$ nanoparticles were synthesized by the chemical co-precipitation technique, using the formula $Co_xFe_{3-x}O_4$ ($0.2 \le x \le 0.8$). Cobalt nitrate and ferric chloride were separately dissolved in 25 mL of deionized water, homogenized via magnetic stirring for 15 minutes, and then combined. Aqueous ammonia was added dropwise to the resultant solution until a stable pH 9 was achieved, forming a brown precipitate.

The mixture was continuously agitated for an additional 15 minutes to ensure complete stoichiometric precipitation. The precipitate was dried at 70–90 ^{o}C for 2 hours, then thermally treated and calcined in ceramic crucibles at 550 ^{o}C for 3 hours. Subsequently, the samples were precisely pulverized in an agate mortar to produce fine powders suitable for characterization and biological evaluation. Antibacterial assays, adhering to established biosafety protocols, using non-clinical reference strains of *E. coli* and *S. aureus*, were conducted in suitable laboratory settings.

2.1.1 Antibacterial Activity Evaluation:

The antibacterial activity of $Co_xFe_{3-x}O_4$, nanoparticles was evaluated against *E. coli* (ATCC 10336), and Stap. aureus (ATCC 29213), obtained from Al-Razi Cether Research and Production of Medical Diagnostic Kits, using the agar well diffusion method. Bacterial suspensions adjusted to the 0.5 McFarland standard were spread onto Mueller-Hinton Agar plates, and 50 μL of nanoparticle suspension 25 mg.mL^{-1} was

loaded into 6 mm wells punched in the agar. After incubation at 37 ^{o}C for 24 h, antibacterial activity was determined by measuring the inhibition zone diameters (mm).

2.1.2 Characterization:

A collection of four samples was synthesized according to the chemical formula $Co_xFe_{3-x}O_4$, with varying cobalt concentrations 0.2 x 0.8, using the co-precipitation technique. The structural characteristics were analyzed by X-ray diffraction using monochromatic Cu Kα, radiation (λ=1.540) from Bruker (Germany) operating over a 2θ range of (9–80$_o$). The surface morphologies were investigated by FESEM (FEI Company, USA), while their elemental composition was determined using the attached EDX. Fourier-transform infrared (FTIR) spectroscopy (from Shimadzu, Japan) was employed to determine the chemical bonding and characteristic vibrational patterns of the materials over the range 4000-400 cm^{-1}. The magnetic properties were measured using a VSM (Lake Shore Cryotronics, USA). The antibacterial efficacy of the produced nanocomposites was assessed using the agar well diffusion technique.

2.2 Results and Discussions:

2.2.1 XRD Analysis:

Figure 1 shows the X-ray diffraction patterns of ($Co_xFe_{3-x}O_4$) nanoparticles synthesized with different cobalt concentrations ($0.2 \le x \le 0.8$). The sample doped with (x=0.2) exhibits a polycrystalline hematite (α-Fe_2O_3) structure as a dominant phase alongside, a minor CoF2O4 phase, confirmed by the presence of distinct peaks related to the crystal planes (012), (104), (110), (113), (024), (116), and (300). These reflections correspond to the rhombohedral structure of the hematite phase according to (JCPDS card 00-024-0072).

The dominance of this phase suggests that the concentration of Co^{2+} is insufficient to form the spinel structure; instead, it enters as a partial substitutional impurity within the Fe_2O_3 structure, leading to the formation of the α-Fe_2O_3 phase [21]. As the cobalt content increases to x = 0.4–0.6, a complete phase transformation into a cubic spinel structure is observed. The diffractograms reveal specific peaks at (440), (511), (422), (400), (311), (220), and (222) which perfectly match $CoFe_2O_4$ phase as noted in (JCPDS:01-086-2267). At these ratios, the peaks characteristic of the hematite phase disappeared, indicating that the prepared powder consisted entirely of phase-pure cobalt ferrite.

This transition is attributed to the stoichiometric balance allowing Co^{2+} / Fe^{3+} ratio and its distribution within tetrahedral (A) and octahedral (B) sites of the spinel lattice. These results indicate the phase transition from α-Fe_2O_3 to $CoFe_2O_4$ as the cobalt content increases. Furthermore, the peaks in sample x = 0.6 were broader than those in x = 0.4, demonstrating that increasing the cobalt content reduces the crystallite size [22], [15]. The average crystallite size for each sample was determined using the Debye–Scherrer equation applied to several prominent diffraction peaks. [23].

$$D = \frac{K\lambda}{\beta cos\theta} \tag{1}$$

where Dp is the crystallite size, β is the full width at half maximum (FWHM), λ is the wavelength of CuK radiation (λ = 1.54A^{o}), and θ is the Bragg angle. With an increased proportion of Co^{2+}, content to (x =0.8), the Co_3O_4 phase becomes dominant. This resulted from an excess of cobalt ions exceeding, the spinel structure's capacity, leading to the separation of the Co_3O_4 phase. Therefore, these results indicate that the formation of the spinel phase depends on the Co/Fe ratio in the initial solution; the $CoFe_2O_4$ phase is formed when the ratio is between x = 0.4–0.6, whereas at x = 0.8 the structure transforms toward the (Co_3O_4) phase, when at lower ratios the powder consists of hematite or of α-Fe_2O_3 doped with cobalt ions. These findings are consistent with previous reports by L.T. Teixeira et al. [24], in which the coexistence of $CoFe_2O_4$ and α-Fe_2O_3 phases was found to depend on the composition and synthesis conditions.

Similarly, B. J. Rani et al. [25] reported that the formation of the spinel phase is strongly influenced by the synthesis method, particularly in co-precipitation systems. A decrease in the lattice constant was observed for cobalt ferrite (a ≈ 8.210 ± 0.005) up to cobalt oxide (a ≈ 8.056) with increasing cobalt ion concentration. This is due to the substitution of iron (III) ions (Fe^{3+}) by cobalt (II) ions (Co^{2+}), which have a smaller ionic radius, resulting in lattice stress and the formation of secondary phases that alter the unit-cell dimensions [26]. The corresponding lattice parameter values are presented in Table 1.

2.3 FTIR Analysis:

The FTIR spectra of the produced $Co_xFe_{3-x}O_4$-based nanoparticle samples reveal changes in the vibrational peaks, which correspond to the phase structure shown in Figure 2. Peaks in the range of about 420 to 664 cm^{-1} in sample (a) indicate that the Fe–O and (Co, Fe)–O bonds are vibrating. This means that there is an impure spinel phase, and the $\alpha - Fe_2O_5$ phase may also be present [27]. Sample (b) exhibits two separate peaks at approximately 420–668 cm^{-1}, corresponding to the vibrations of the metal-oxygen (M–O), bonds at the tetrahedral (A-site) and octahedral (B-site) locations inside the spinel structure. This validates the development of the spinel $CoFe_2O_4$ phase [28], [29].

In sample (c), the same ferrite peaks were observed; however, they exhibited a slight shift to approximately 807–420 cm^{-1}. This means there is a cobalt oxide phase without occupying the spinel structure. The bands at 3407 and 1389 cm^{-1} are thought to be due to the H-O-H bond in adsorbed water molecules, which are expanding. FTIR spectroscopy

Table 1. The Structural parameters of $Co_xFe_{3-x}O_4$ nanoparticles at different cobalt concentrations ($0.2 \leq x \leq 0.8$).

Composition	Crystallite Size (nm)	a_exp ()	Lattice Strain (ε)	Error %
a (x = 0.2)	20.70	—	-0.007	0.76
b (x = 0.4)	16.81	8.210	-0.014	1.47
c (x = 0.6)	15.88	8.203	-0.007	0.75
d (x = 0.8)	11.88	8.056	-0.004	0.41

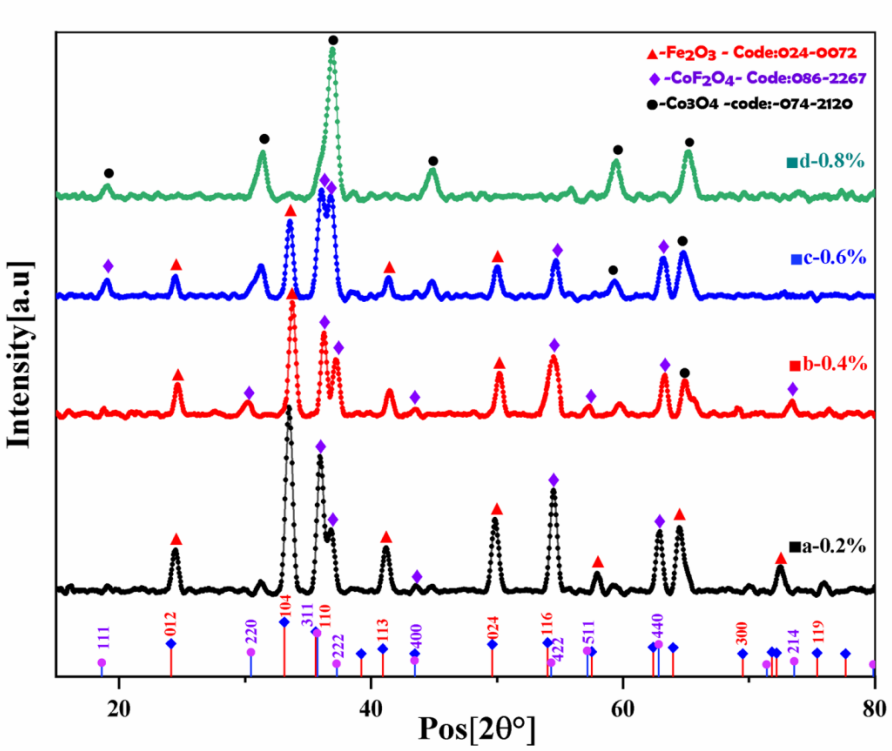

Figure 1. X-ray diffraction patterns of the synthesized nanoparticles at different cobalt concentrations: (a) x = 0.2, (b) x = 0.4, (c) x = 0.6, and (d) x = 0.8.

indicated that samples (b) and (c) contain the spinel structure of $CoFe_2O_4$ with varying degrees of purity. These results agree with previous reports [30].

2.3.1 FESEM and EDX analysis:

Using energy-dispersive X-ray spectroscopy (EDX), Figure 3 shows the chemical and structural analysis of the prepared $Co_xFe_{3-x}O_4$-based nanoparticle samples. The cobalt content increases, according to the formula ($0.2 \leq x \leq 0.8$), as the value of x increases, indicating the successful substitution of Fe+3 ions with Co^{+2} ions in the crystal lattice of the samples. This analysis confirms the presence of the main elements (Fe, Co, and O), consistent with the cobalt spinel ferrite structure. Because the compound is highly effective at absorbing oxygen, it may exhibit a high adsorption capacity [31]. The secondary peaks of (Au), which are created by coating the samples for microscopic study, also include trace amounts of other elements such as (Cl, Ca, and Mn), as shown in Figure 3. Although they are believed to be caused by impurities in the materials used or by the laboratory preparation procedures, these traces do not affect the primary phase [32].

Figure 4. FESEM micrographs of $Co_xFe_{33}O_4$ nanoparticles at different cobalt concentrations ($0.2 \leq x \leq 0.8$) show a semi-spherical shape. Some agglomeration is visible due to magnetic interaction forces. According to the attached graphs (A-D), there is a regular decrease in particle size from (~71 ± 5nm at x=0.2 to ~49 ± 3 nm at x = 0.8), as reported previously [33]. This decrease is physically explained by Co^{+2} slowing grain growth and increasing the number of nucleation sites during the reaction [34]. This enhances nucleation, leading to smaller, more homogeneous particles [35].

FESEM particle sizes (49–71 nm), are larger than XRD crystallite sizes (14–21 nm), due to agglomeration of smaller

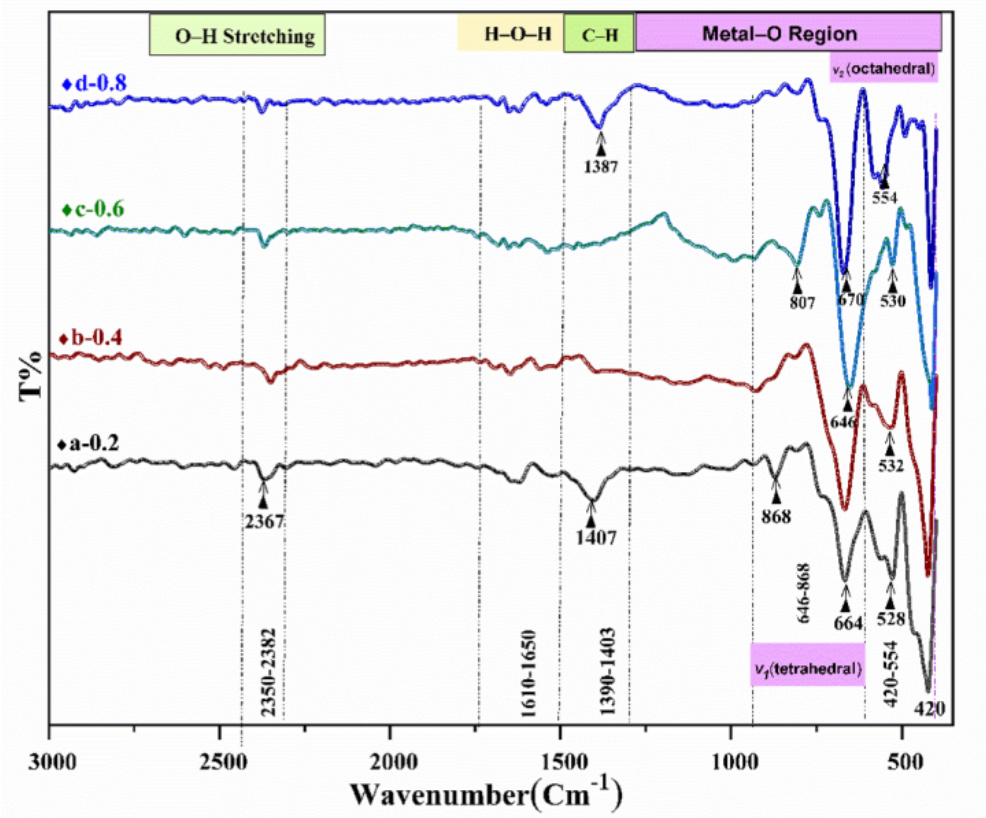

Figure 2. FTIR spectra of nanoparticles with varying compositions: (a) x = 0.2, (b) x = 0.4, (c) x = 0.6, and (d) x = 0.8.

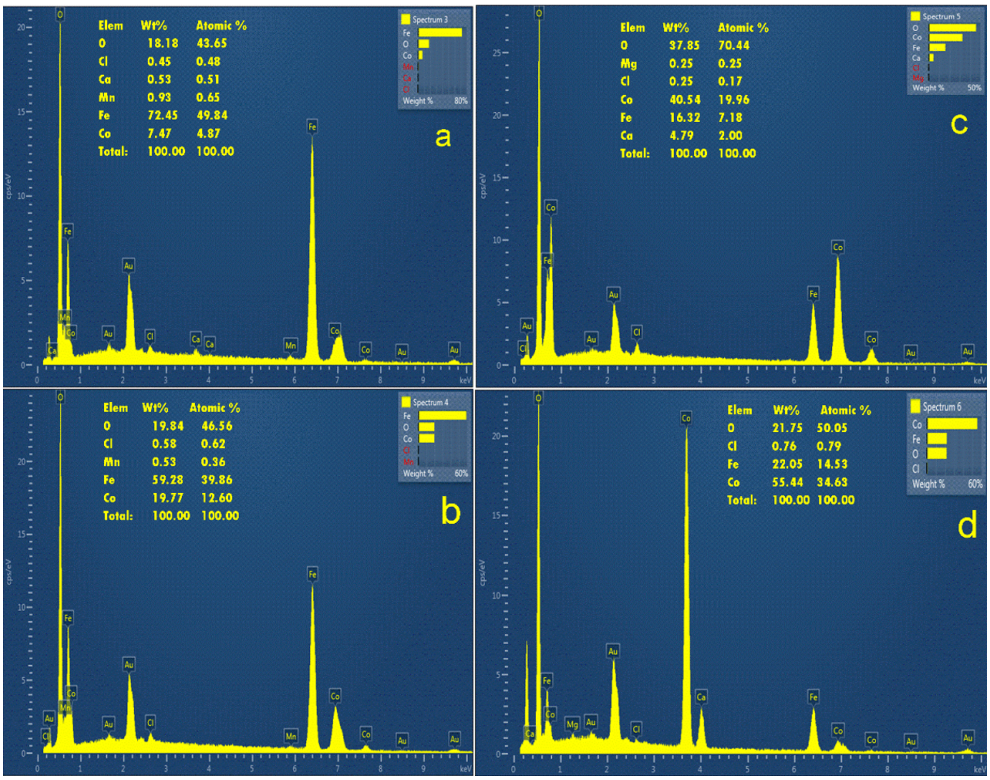

Figure 3. EDX spectra of nanoparticles with varying compositions: (a) x = 0.2, (b) x = 0.4, (c) x = 0.6, and (d) x = 0.8.

crystallites into larger particles [36]. The transition to smaller sizes increases the effective surface area. The irregular nanoparticle distribution on the surface results from variations in cation distribution between tetrahedral and octahedral sites in the spinel structure, driven by differences in the (Co/Fe) ratio. Preparation conditions, temperature, crystal growth mechanism, and pH influence lead to non-uniform particle distribution [37].

2.3.2 Magnetic Properties:

The VSM was used to analyze the magnetic properties of $Co_xFe_{3-x}O_4$-based nanoparticles ($0.2 \leq x \leq 0.8$), as shown in Figure 5. The M-H curves of the prepared samples show that the gradual substitution of Co^{2+} ions in the cobalt-iron ferrite leads to a modification in the magnetic properties. This is mainly due to the increase in crystalline anisotropy associated with the unquenched orbital moment of the Co^{2+} ions located in octahedral positions.

The nonlinear behavior (Ms) and (nB) accurately represent how cations are distributed across tetrahedral and octahedral sites, leading to changes in the strength of the A–B superexchange interactions and consequently affecting the magnetic properties of the nanoparticles [38]. The sample with composition X = 0.4 shows the highest values of Mr and K, which indicates the achievement of the best magnetic stability and stronger interaction between molecules. Conversely, the low values of Mr in the other samples indicate relatively softer magnetic behavior owing to nanoscale effects. However, the finite coercive force and remanent magnetization observed in all samples confirm that the nanoparticles remain in a magnetically blocked ferrimagnetic state [39].

The variation in (Hc) values underscores the crucial role of crystalline anisotropy in counteracting size effects. The present results, align with those reported by Sangsuriyonk et al. [40] for $Co_xFe_{12}O_4$, nanoparticles synthesized, via co-precipitation. An increase in Co^{2+}, content led to elevated Hc, and Mr values confirming ferrimagnetic behavior. This finding is consistent with the magnetically blocked ferrimagnetic state observed in the current study. The moment (nB) was calculated, using the following equation [41], [42].

$$nB = \frac{Mw \times Ms}{5588} \tag{2}$$

where Mw is the molecular weight ($g \cdot mol^{-1}$), Ms is the saturation magnetization ($emu \cdot g^{-1}$), and 5585 is a constant. The magnetic moments indicate that all the samples exhibit ferromagnetism. The following equation calculates the K-anisotropy constant [43], [44].

$$K = \frac{Ms \times Hc}{0.98} \tag{3}$$

The concentration of the substituted ion influences the anisotropy constant. That is, the variation constant increases with cobalt content. Where K is the anisotropy constant, Ms is the saturation magnetization, Hc is the coercivity field, and 0.98 is a constant factor.

Table 2. Magnetic properties of $Co_xFe_{3-x}O_4$ nanoparticle at different cobalt concentrations (x = 0.2, 0.4, 0.6, and 0.8).

Sample	(Ms)(emu/g)	(Mr)(emu/g)	(Hc)(Oe)	(nB)(μB)	(K)(erg/g)
a	0.145	0.050	1903	0.0060	287
b	2.512	1.00	1398	0.105	3657
c	2.037	0.062	350	0.086	740
d	0.109	0.033	1911	0.0046	217

2.4 Antibacterial activities:

The antibacterial activities of the $Co_xFe_{3-x}O_4$-based nanoparticles were tested against selected microbes, including *E. coli* and *S. aureus.* Antibacterial activity against *E. coli* and *S. aureus* was tested using the agar well diffusion method (30 $mg.mL^{-1}$). Inhibition zones were measured after 24 hours of incubation at 37^oC to ensure reproducibility. These strains were chosen as models of common bacterial pathogens that infect the community and can be ingested through contaminated water.

Figure 6 and Table 3 show that a concentration of 30 $mg.mL^{-1}$ of synthesized COFNPs, CO_3O_4_COFNPs, and CO_3O_4 nanoparticles resulted in strong antibacterial activity against *S. aureus* and *E. coli*, with mean inhibition diameters of 24±1mm, consistent with previous studies [45]. All measurements were performed on three independent samples. No significant differences were found between G-negative and G-positive bacteria. This similarity suggests that the inhibition mechanism depends on the nanoparticles' immediate surface effect rather than on differences in cell wall composition [46].

A slight increase in the inhibition zone with increasing cobalt concentration may lead to improved surface catalytic activity of the two-phase system and increased generation of reactive oxygen species (ROS). Moreover, Co^{2+} ions may interfere with cell membrane permeability and inhibit intracellular metabolic processes. The presence of a secondary phase, such as Co_3O_4, additionally enhances the interaction between the substance and the bacteria [21], [47]. Table 4 presents an overview of the structural, magnetic, and antibacterial characteristics of the produced $Co_xFe_{3-x}O_4$ nanoparticles.

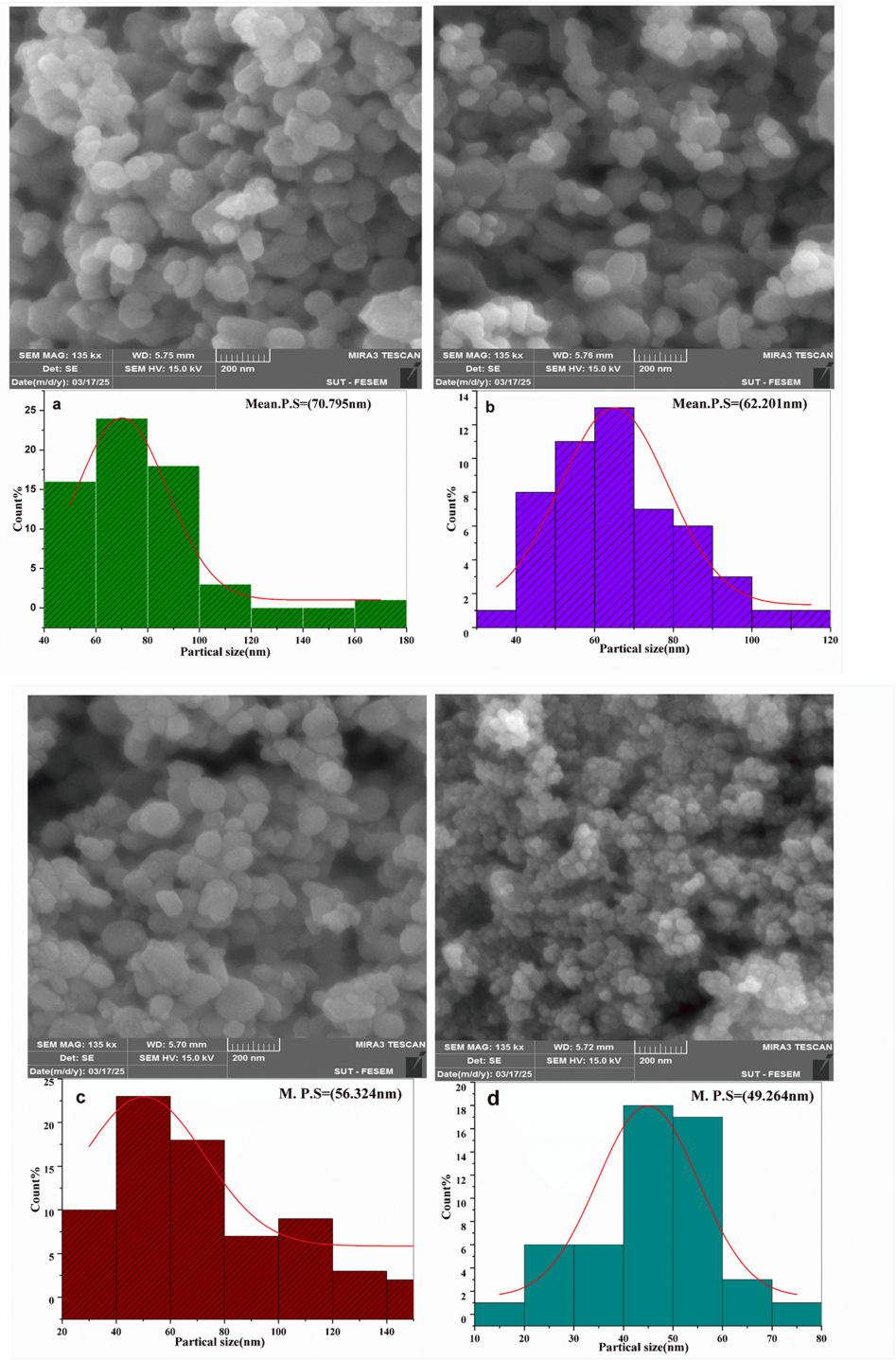

Figure 4. FESEM micrographs of $Co_xFe_{3-x}O_4$ nanoparticles at different cobalt concentrations: (a) x = 0.2, (b) x = 0.4, (c) x = 0.6, and (d) x = 0.8. All images were recorded with a scale bar of 200 nm.

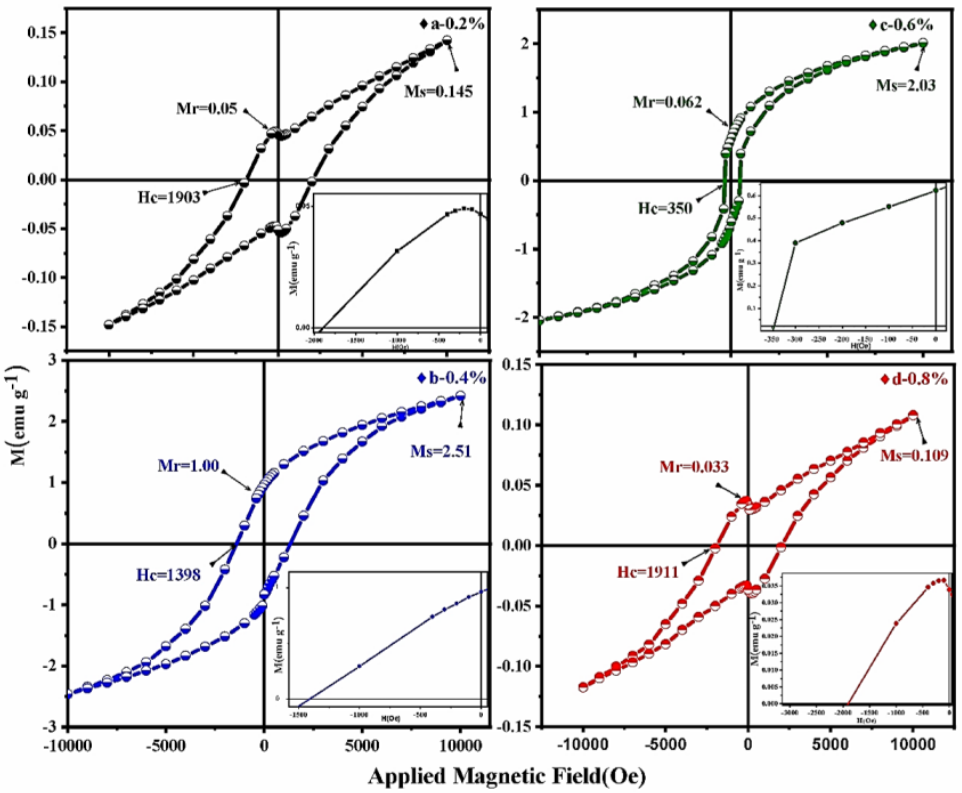

Figure 5. Magnetic hysteresis (M–H) loops of $Co_xFe_{3-x}O_4$ nanoparticles with various cobalt concentrations (a) x = 0.2, (b) x = 0.4, (c) x = 0.6, and (d) x = 0.8.

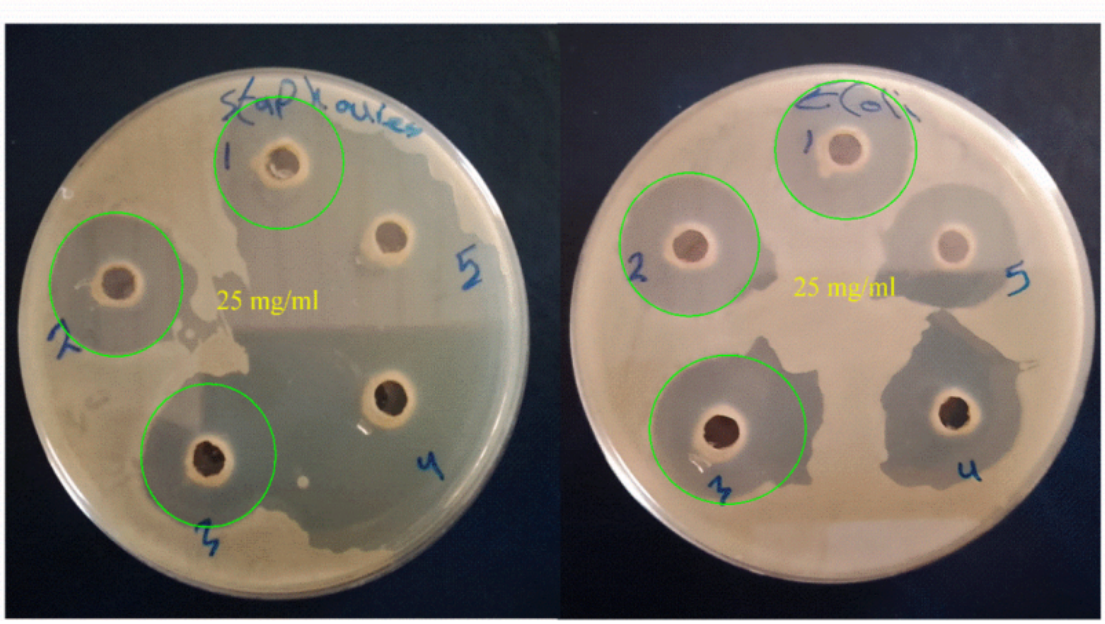

Figure 6. Antibacterial activity of as-synthesized materials against *E. coli* (Negative Strain) and *Staph. aureus* (Positive Strain).

Table 3. Antibacterial activity results expressed as zone of inhibition (ZOI), diameters (mm) for all prepared samples.

Exp.No.	Sample	Gram-negative (*E. coli*) (mm)	Gram-positive (*Staph. aureus*) (mm)
1	CoF	24	24
2	CoF/CoO	25	24
3	Co_3O_4	25	24

Table 4. Summary of structural, magnetic, and antibacterial properties of $Co_xFe_{3-x}O_4$ nanoparticles.

(Co-content) x	Phase Composition	Crystallite Size (nm)	Particle Size (nm)	Ms (emu/g)	Hc (Oe)	ZIO (mm)
0.2	α-Fe_2O_3	20.70	~71	0.145	1903	
0.4	$CoFe_2O_4$	16.81	~60	2.51	1398	24–25
0.6	$CoFe_2O_4$	15.88	~55	2.03	350	25
0.8	Co_3O_4	11.88	~49	0.109	1911	24

3. Conclusion:

In this study, $Co_xFe_{3-x}O_4$ nanoparticles were prepared by the co-precipitation method, with the cobalt ratio varied. FTIR and XRD analyses showed that the crystalline phase depends mainly on the Co/Fe ratio, with the (α-Fe_2O_3) phase appearing at low ratios. Spinel $CoFe_2O_4$ forms at medium ratios, and the Co_3O_4 phase appears at high ratios. It was found that the size of crystals and nanoparticles decreases with increasing wt.Co%, due to the inhibition of grain growth and an increase in nucleation sites. Magnetic properties were also affected by particle size, cation distribution, phase integrity, and the tendency toward superparamagnetic behavior at small nanoscale dimensions. The synthesized nanoparticles demonstrated significant antibacterial activity, likely attributable to their increased surface area, phase heterogeneity, and the potential generation of reactive oxygen species. These findings highlight the multifunctional potential of ($Co_xFe_{3-x}O_4$) nanoparticles for biomedical applications, particularly as antibacterial agents, magnetic materials, and targeted drug-delivery agents. Subsequently, research should concentrate on optimising synthesis conditions to improve crystalline purity and on assessing in vivo effectiveness for advanced medicinal applications.

Funding: This investigation is conducted as an independent research initiative without external financial support.

Data Availability Statement: All of the data supporting the findings of the presented study are available at the corresponding author.

Declarations:

Conflict of interest: The authors confirm that there is no conflict of interest.

Ethical approval: The research team affirms that no conflicts of interest, financial or otherwise.

Author Contributions: Thair Q. Jassim conducted the experiments, analyzed the data, and wrote the manuscript. Q. Noufan Abdullah conceived the study, supervised the research.

References

[1] Zhikai Yan, Jianming Gao, Yang Li, Mei Zhang, and Min Guo. Hydrothermal synthesis and structure evolution of metal-doped magnesium ferrite from saprolite laterite. *RSC advances*, 5(112):92778–92787, 2015, doi:10.1039/C5RA17145H.

[2] Qing Song, Yong Ding, Zhong Lin Wang, and Z John Zhang. Tuning the thermal stability of molecular precursors for the nonhydrolytic synthesis of magnetic mnfe2o4 spinel nanocrystals. *Chemistry of Materials*, 19(19):4633–4638, 2007, doi:10.1021/cm070990o.

[3] Vinod Kumar, Anu Rana, MS Yadav, and RP Pant. Size-induced effect on nano-crystalline cofe2o4. *Journal of Magnetism and Magnetic Materials*, 320(11):1729–1734, 2008, doi:10.1016/j.jmmm.2008.01.021.

[4] K Raj, B Moskowitz, and S Tsuda. New commercial trends of nanostructured ferrofluids. *Indian J. Eng. Mater. Sci*, 11:241–252, 2004.

[5] M Grigorova, HJ Blythe, V Blaskov, V Rusanov, V Petkov, V Masheva, D Nihtianova, Ll M Martinez,

JS Munoz, and M Mikhov. Magnetic properties and mössbauer spectra of nanosized cofe2o4 powders. *Journal of magnetism and magnetic materials*, 183(1-2):163–172, 1998, doi:10.1016/S0304-8853(97)01031-7.

[6] AE Berkowitz and WJ Schuele. Magnetic properties of some ferrite micropowders. *Journal of Applied Physics*, 30(4):S134–S135, 1959, doi:10.1063/1.2185853.

[7] Thomas Dippong, Oana Cadar, Erika Andrea Levei, Iosif-Grigore Deac, and Gheorghe Borodi. Formation of cofe2o4/pva-sio2 nanocomposites: effect of diol chain length on the structure and magnetic properties. *Ceramics International*, 44(9):10478–10485, 2018, doi:10.1016/j.ceramint.2018.03.065.

[8] Behrooz Shahbahrami, Sayed Mahmood Rabiee, and Reza Shidpoor. Effect of ph value on synthesis and properties of zinc cobalt ferrite nano powders prepared via co-precipitation method. *Research Square*, 2020, doi:10.21203/rs.3.rs-28190/v1.

[9] Feng Huixia, Chen Baiyi, Zhang Deyi, Zhang Jianqiang, and Tan Lin. Preparation and characterization of the cobalt ferrite nano-particles by reverse coprecipitation. *Journal of magnetism and magnetic materials*, 356:68–72, 2014, doi:10.1016/j.jmmm.2013.12.033.

[10] Y Chen, M Ruan, YF Jiang, SG Cheng, and W Li. The synthesis and thermal effect of cofe2o4 nanoparticles. *Journal of Alloys and Compounds*, 493(1-2):L36–L38, 2010, doi:10.1016/j.jallcom.2009.12.170.

[11] GSN Rao, OF Caltun, KH Rao, PSV Subba Rao, and B Parvatheeswara Rao. Improved magnetostrictive properties of co-mn ferrites for automobile torque sensor applications. *Journal of magnetism and magnetic materials*, 341:60–64, 2013, doi:10.1016/j.jmmm.2013.04.039.

[12] SC Goh, CH Chia, S Zakaria, M Yusoff, CY Haw, Sh Ahmadi, NM Huang, and HN Lim. Hydrothermal preparation of high saturation magnetization and coercivity cobalt ferrite nanocrystals without subsequent calcination. *Materials Chemistry and Physics*, 120(1):31–35, 2010, doi:10.1016/j.matchemphys.2009.10.016.

[13] AK Giri, EM Kirkpatrick, P Moongkhamklang, SA Majetich, and VG Harris. Photomagnetism and structure in cobalt ferrite nanoparticles. *Applied physics letters*, 80(13):2341–2343, 2002, doi:10.1063/1.1464661.

[14] M Sajjia, Mohamed Oubaha, M Hasanuzzaman, and AG Olabi. Developments of cobalt ferrite nanoparticles prepared by the sol-gel process. *Ceramics International*, 40(1):1147–1154, 2014, doi:10.1016/j.ceramint.2013.06.116.

[15] Khalid Mujasam Batoo, Dina Salah, Gagan Kumar, Arun Kumar, Mahavir Singh, M Abd El-Sadek, Feroz Ahmad Mir, Ahamad Imran, and Daler Adil Jameel. Hyperfine interaction and tuning of magnetic anisotropy of cu doped cofe2o4 ferrite nanoparticles. *Journal of Magnetism and Magnetic Materials*, 411:91–97, 2016, doi:10.1016/j.jmmm.2016.03.058.

[16] Mahboubeh Houshiar, Fatemeh Zebhi, Zahra Jafari Razi, Ali Alidoust, and Zohreh Askari. Synthesis of cobalt ferrite (cofe2o4) nanoparticles using combustion, coprecipitation, and precipitation methods: A comparison study of size, structural, and magnetic properties. *Journal of Magnetism and Magnetic Materials*, 371:43–48, 2014, doi:10.1016/j.jmmm.2014.06.059.

[17] K Maaz, S Karim, A Mashiatullah, J Liu, MD Hou, YM Sun, JL Duan, HJ Yao, D Mo, and YF Chen. Structural analysis of nickel doped cobalt ferrite nanoparticles prepared by coprecipitation route. *Physica B: Condensed Matter*, 404(21):3947–3951, 2009, doi:10.1016/j.physb.2009.07.134.

[18] Thomas Dippong, Erika Andrea Levei, Gheorghe Borodi, Firuta Goga, and Lucian Barbu Tudoran. Influence of co/fe ratio on the oxide phases in nanoparticles of coxfe3-xo4. *Journal of Thermal Analysis and Calorimetry*, 119(2):1001–1009, 2015, doi:10.1007/s10973-014-4280-7.

[19] Davood Gheidari, Morteza Mehrdad, Saloomeh Maleki, and Samanesadat Hosseini. Synthesis and potent antimicrobial activity of cofe2o4 nanoparticles under visible light. *Heliyon*, 6(10), 2020, doi:10.1016/j.heliyon.2020.e05058.

[20] Mayank Bhushan, Yogesh Kumar, Latha Periyasamy, and Annamraju Kasi Viswanath. Antibacterial applications of α-fe2o3/co3o4 nanocomposites and study of their structural, optical, magnetic and cytotoxic characteristics. *Applied Nanoscience*, 8(1):137–153, 2018, doi:10.1007/s13204-018-0656-5.

[21] Lilia Ajroudi, Sylvie Villain, V Madigou, N Mliki, and Ch Leroux. Synthesis and microstructure of cobalt ferrite nanoparticles. *Journal of Crystal Growth*, 312(16-17):2465–2471, 2010, doi:10.1016/j.jcrysgro.2010.05.024.

[22] Vijaykumar V Paike, Prashant S Niphadkar, Vijay V Bokade, and Praphulla N Joshi. Synthesis of spinel cofe2o4 via the co-precipitation method using tetraalkyl ammonium hydroxides as precipitating agents. *Journal of the American Ceramic Society*, 90(9):3009–3012, 2007, doi:10.1111/j.1551-2916.2007.01843.x.

[23] Lunhong Ai and Jing Jiang. Influence of annealing temperature on the formation, microstructure and magnetic properties of spinel nanocrystalline cobalt ferrites. *Current Applied Physics*, 10(1):284–288, 2010, doi:10.1016/j.cap.2009.06.007.

[24] Lucas Tonetti Teixeira, Marcos Medeiros, Liying Liu, Vinicius Novaes Park, Célio Valente-Rodriguez, So-

nia Letichevsky, Humberto Vieira Fajardo, Rogério Navarro Correia de Siqueira, Marcelo Eduardo Huguenin Maia da Costa, and Amilton Barbosa Botelho Junior. Sustainable synthesis of cofe2o4/fe2o3 catalyst for hydrogen generation from sodium borohydride hydrolysis. *Catalysts*, 15(10):943, 2025, doi:10.3390/catal15100943.

[25] B Jansi Rani, M Ravina, B Saravanakumar, G Ravi, V Ganesh, S Ravichandran, and R Yuvakkumar. Ferrimagnetism in cobalt ferrite (cofe2o4) nanoparticles. *Nano-Structures & Nano-Objects*, 14:84–91, 2018, doi:10.1016/j.nanoso.2018.01.012.

[26] R Sagayaraj, S Aravazhi, C Selva Kumar, S Senthil Kumar, and G Chandrasekaran. Tuning of ferrites (coxfe3-xo4) nanoparticles by co-precipitation technique. *SN Applied Sciences*, 1(3):271, 2019, doi:10.1007/s42452-019-0244-7.

[27] Farahmandjou M. and Soflaee F. Low temperature synthesis of $\alpha - fe_2o_3$ nanorods. *World Journal of Condensed Matter Physics*, 4:131–135, 2014, doi:10.7508/jns.2014.04.002.

[28] Annie Vinosha, Emima Jeronsia, Alison christina Fernandez, Jerome Das, et al. Investigation of optical, electrical and magnetic properties of cobalt ferrite nanoparticles by naive co-precipitation technique. *Optik*, 127(20):9917–9925, 2016, doi:10.1016/j.ijleo.2016.07.063.

[29] Augustin Joseph, Balu Thangaraj, s Rejith, and A. Anto Arockia Raj. Synthesis and characterization of cobalt ferrite magnetic nanoparticles coated with polyethylene glycol. *Advanced Nano Biology Medicine*, pages 71–77, 01 2017.

[30] A Karthikeyan, R Mariappan, R Bakkiyaraj, and E Krishnamoorthy. High electrochemical performance of co3o4-pvdf-nmp-based supercapacitor electrode. *Journal of Materials Science: Materials in Electronics*, 34(8):728, 2023, doi:10.1007/s10854-023-10147-w.

[31] Liufang Yang, Yongan Xie, Heyun Zhao, Xinghui Wu, and Yude Wang. Preparation and gas-sensing properties of nife2o4 semiconductor materials. *Solid-state electronics*, 49(6):1029–1033, 2005, doi:10.1016/j.sse.2005.03.022.

[32] LTH Phong, DH Manh, PH Nam, VD Lam, BX Khuyen, BS Tung, TN Bach, DK Tung, NX Phuc, TV Hung, et al. Structural, magnetic and hyperthermia properties and their correlation in cobalt-doped magnetite nanoparticles. *RSC advances*, 12(2):698–707, 2022, doi:10.1039/d1ra07407e.

[33] Varzaneh A. G. Kameli P. Mosleh Z., Beygmohammadvand M. Influence of cobalt substitution in $cofe_2o_4$ nanoparticles. *Heliyon*, 11(1), 2025, doi:10.1016/j.heliyon.2024.e41276.

[34] M Hussain, A Mehmood, F Ali, ZA Sandhu, MA Raza, S Sajid, M Sohaib, MT Khan, AH Bhalli, A Hussain, et al. Tuning the magnetic behavior of zinc ferrite via cobalt substitution: A structural analysis. acs omega 9: 2536-2546, 2024, , doi:10.1021/acsomega.3c07251.

[35] WS Mohamed, Meshal Alzaid, Mohammed SM Abdelbaky, Zakariae Amghouz, Santiago García-Granda, and Ahmed M. Abu-Dief. Impact of co2+ substitution on microstructure and magnetic properties of coxzn1-xfe2o4 nanoparticles. *Nanomaterials*, 9(11):1602, 2019, doi:10.3390/nano9111602.

[36] Shahid Ahmad Shah, Hamnesh Mahajan, Rupam Mukherjee, Deepak Basandrai, and Owais Amin. Role of annealing on structural and magnetic properties of mg-zn spinel ferrite nanoparticles. *Journal of Sol-Gel Science and Technology*, pages 1–8, 2025, doi:10.1007/s10971-025-07011-0.

[37] Zhigang Zhang, Yihan Liu, Guangchun Yao, Guoyin Zu, and Yi Hao. Synthesis and characterization of nife2o4 nanoparticles via solid-state reaction. *International Journal of Applied Ceramic Technology*, 10(1):142–149, 2013, doi:10.1111/j.1744-7402.2011.02719.x.

[38] Rohit Jasrotia, Jyoti Prakash, Yasser B Saddeek, Abdullah H Alluhayb, Alaa M Younis, Natrayan Lakshmaiya, Chander Prakash, KA Aly, Mika Sillanpää, Yasser AM Ismail, et al. Cobalt ferrites: Structural insights with potential applications in magnetics, dielectrics, and catalysis. *Coordination Chemistry Reviews*, 522:216198, 2025, doi:10.1016/j.ccr.2024.216198.

[39] Alexander Omelyanchik, María Salvador, Franco D'orazio, Valentina Mameli, Carla Cannas, Dino Fiorani, Anna Musinu, Montserrat Rivas, Valeria Rodionova, Gaspare Varvaro, et al. Magnetocrystalline and surface anisotropy in cofe2o4 nanoparticles. *Nanomaterials*, 10(7):1288, 2020, doi:10.3390/nano10071288.

[40] Kittipon Sangsuriyonk, Nophawan Paradee, Kornkanok Rotjanasuworapong, and Anuvat Sirivat. Synthesis and characterization of coxfe1- xfe2o4 nanoparticles by anionic, cationic, and non-ionic surfactant templates via co-precipitation. *Scientific reports*, 12(1):4611, 2022, doi:10.1038/s41598-022-08709-9.

[41] Ahmad Amirabadizadeh and Tyebeh Amirabadi. Effect of substitution of al for fe on magnetic properties and particle size of ni-co nanoferrite. *World J. Condens. Matter Phys.*, 3(3):131–135, 2013, doi:10.4236/wjcmp.2013.33021.

[42] Mark Fox. *Optical properties of solids*, volume 3. Oxford university press, 2010.

[43] Sunil M Patange, Sagar E Shirsath, Santosh S Jadhav, and Kamalakar M Jadhav. Cation distribution study of

nanocrystalline nife2- xcrxo4 ferrite by xrd, magnetization and mössbauer spectroscopy. *physica status solidi (a)*, 209(2):347–352, 2012, doi:10.1002/pssa.201127232.

[44] Geeta Rana and Umesh C Johri. A study on structural and magnetic properties of ni-substituted magnetite nanoparticles. *Journal of alloys and compounds*, 577:376–381, 2013, doi:10.1016/j.jallcom.2013.05.184.

[45] Ahmed M El-Khawaga, Mohamed A Elsayed, Yosri A Fahim, and Rasha E Shalaby. Promising photocatalytic and antimicrobial activity of novel capsaicin coated cobalt ferrite nanocatalyst. *Scientific Reports*, 13(1):5353, 2023, doi:10.1038/s41598-023-32323-y.

[46] Noppakun Sanpo, Cuie Wen, Christopher Berndt, and James Wang. Antibacterial properties of spinel ferrite nanoparticles. *Journal of Applied Microbiology*, 2013.

[47] Nurdan Kurnaz Yetim, Elvan Hasanoğlu Özkan, and Hatice Öğütçü. Use of co3o4 nanoparticles with different surface morphologies for removal of toxic substances and investigation of antimicrobial activities via in vivo studies. *Environmental Science and Pollution Research*, 30(48):106585–106597, 2023, doi:10.1007/s11356-023-29879-7.

تأثير نسبة $Co:Fe$ على التحولات الطورية والخواص التركيبية والمغناطيسية والمضادة للبكتيريا لمركبات $Co_xFe_{3-x}O_4$ النانوية المحضرة بطريقة بطريقة الترسيب المشترك

ثائر قحطان جاسم * ، قحطان نوفان عبدالله

قسم الفيزياء، كلية التربية للعلوم الصرفة، جامعة تكريت، تكريت، العراق.

* الباحث المسؤول: *thairr112@gmail.com*

الخلاصة

في هذه الدراسة، تم تحضير جسيمات $Co_xFe_{3-x}O_4$ النانوية بتراكيز مختلفة من الكوبالت ($0.2 \le x \le 0.8$) باستخدام طريقة الترسيب المشترك بخطوة واحدة بسيطة. تمت دراسة تأثير إحلال الكوبالت على الخصائص التركيبية والمورفولوجية والمغناطيسية والمضادة للبكتيريا باستخدام حيود الأشعة السينية (*XRD*)، والمجهر الإلكتروني الماسح بالانبعاث الميداني (*FESEM*)، والتحليل الطيفي للأشعة السينية المشتتة للطاقة (*EDX*)، وتحليل الأشعة تحت الحمراء بتحويل فورييه (*FTIR*)، وجهاز قياس المغناطيسية بالعينة المهتزة (*VSM*).

أظهرت النتائج تكوّن البنية الإسبنيلية المكعبة عند التراكيز المتوسطة، مع أحجام بلورية تراوحت بين 14 و 21 نانومتر. كما لوحظ ظهور أطوار ثانوية شملت الهيماتيت ($\alpha-Fe_2O_3$) وأكاسيد الكوبالت (CoO/Co_3O_4). أكد تحليل *EDX* التركيب العنصري والتوزيع شبه المتجانس للعناصر، في حين بيّنت أطياف *FTIR* الاهتزازات المميزة لروابط المعدنالأوكسجين في البنية الإسبنيلية.

أظهرت القياسات المغناطيسية عند درجة حرارة الغرفة قيم مغنطة إشباع تراوحت بين 0.109 و 2.51 *emu/g* ، مما يدل على سلوك فوق بارامغناطيسي يُعزى إلى التأثيرات النانوية. أظهرت الجسيمات النانوية نشاطًا مضادًا للبكتيريا، حيث بلغت مناطق التثبيط حتى ٢٥ مم ضد بكتيريا *S. aureus* و *E. coli* ، مما يعزز إمكانية استخدامها في التطبيقات الطبية والتقنية.

الكلمات الدالة : أكسيد الحديد الثلاثي (Fe_2O_3)؛ الأطوار؛ النشاط المضاد للبكتيريا؛ أكسيد الكوبالت (Co_3O_4)؛ الإشريكية القولونية (*E. coli*).

التمويل: جرى هذا البحث كمبادرة بحثية مستقلة دون أي دعم مالي خارجي.

بيان توفر البيانات: جميع البيانات الداعمة لنتائج هذه الدراسة متاحة لدى المؤلف المراسل عند الطلب.

اقرارات:

تضارب المصالح: يؤكد فريق البحث عدم وجود أي تضارب في المصالح، سواء كان مالياً أو غير ذلك.

الموافقة الأخلاقية: لم تتضمن هذه الدراسة أي مشاركين من البشر أو حيوانات.

مساهمات المؤلفين: أجرى ثائر قحطان جاسم التجارب، وحلل البيانات، وكتب المخطوطة. أما قحطان نوفان عبد الله فقد وضع فكرة الدراسة، وأشرف على البحث.